J|A|C|S ARTICLES

Published on Web 02/10/2010

Study of Ion-Paired Iridium Complexes (Soft Salts) and Their Application in Organic Light Emitting Diodes

Chao Wu,[†] Hsiao-Fan Chen,[‡,§] Ken-Tsung Wong,[‡] and Mark E. Thompson*[,†,§]

Department of Chemical Engineering and Materials Science, University of Southern California, Los Angeles, California 90089, Department of Chemistry, National Taiwan University, Taipei 106, Taiwan, and Department of Chemistry, University of Southern California, Los Angeles, California 90089

Received November 22, 2009; E-mail: met@usc.edu

Abstract: Three Ir-based materials were synthesized through metathesis reaction between halide and alkali metal salts of two cationic and three anionic Ir complexes, respectively. The resulting "soft salt" complexes are composed of an organometallic cation and an organometallic anion. The electrochemical and photophysical characterization of these compounds is reported. The redox potentials of the soft salts are shown to be determined by the lowest energy potentials of the two ions. Energy transfer between the ions in solution is observed, and found to take place at diffusion controlled rates. Organic LEDs were prepared with each of the three soft salts, using the simple structure of anode/PVK/soft salt/BCP/cathode. The soft salts yielded maximal external quantum efficiencies (EQE) ranging from 0.2% to 4.7%. The study suggests that the internal energy alignment between two ions in the soft salts is responsible for the widely disparate results. To achieve a high EQE, it is critical to have the HOMO and LUMO values of one of the ions fall between those of the other ion, that is, one ion has both the lowest oxidation potential and the least negative reduction potential.

Introduction

Since the groundbreaking report of heterojunction organic light-emitting diodes (OLED) by Tang et al.,[1] an extensive amount of research interest has been drawn to this field. A marked advance was made in OLED efficiencies when phosphorescent dopants were introduced.[2−8] Among the most successful phosphorescent emitters are cyclometalated Ir complexes due to a number of important features, including strong spin−orbit coupling,[9] which leads to phosphorescent lifetimes in the 1−10 μs range,[5] high phosphorescent efficiencies at room temperature,[10] and good color tunability of the emission energy, spanning the visible spectrum.[11,12] Both neutral and ionic Ir-based complexes have these photophysical properties.[13,14] Neutral Ir-based complexes have been used in OLED structures, consisting of distinct carrier transporting/blocking and emitting layers.[15] Cationic Ir complexes have been used in light-emitting electrochemical cells (LEC), which typically consist of a single active layer, responsible for both carrier transport and light emission,[16−19] while the studies of anionic Ir complexes have been mainly focused on their photophysics.[20−22]

[†] Department of Chemical Engineering and Materials Science, University of Southern California.
[‡] National Taiwan University.
[§] Department of Chemistry, University of Southern California.

(1) Tang, C. W.; VanSlyke, S. A. *Appl. Phys. Lett.* **1987**, *51*, 913–915.
(2) Kwong, R. C.; Sibley, S.; Dubovoy, T.; Baldo, M.; Forrest, S. R.; Thompson, M. E. *Chem. Mater.* **1999**, *11*, 3709–3713.
(3) Adachi, C.; Baldo, M. A.; Forrest, S. R.; Thompson, M. E. *Appl. Phys. Lett.* **2000**, *77*, 904–906.
(4) Baldo, M. A.; O'Brien, D. F.; You, Y.; Shoustikov, A.; Sibley, S.; Thompson, M. E.; Forrest, S. R. *Nature* **1998**, *395*, 151–154.
(5) Baldo, M. A.; Lamansky, S.; Burrows, P. E.; Thompson, M. E.; Forrest, S. R. *Appl. Phys. Lett.* **1999**, *75*, 4–6.
(6) Adachi, C.; Baldo, M. A.; Thompson, M. E.; Forrest, S. R. *J. Appl. Phys.* **2001**, *90*, 5048–5051.
(7) Ikai, M.; Tokito, S.; Sakamoto, Y.; Suzuki, T.; Taga, Y. *Appl. Phys. Lett.* **2001**, *79*, 156–158.
(8) Markham, J. P. J.; Lo, S. C.; Magennis, S. W.; Burn, P. L.; Samuel, I. D. W. *Appl. Phys. Lett.* **2002**, *80*, 2645–2647.
(9) Sprouse, S.; King, K. A.; Spellane, P. J.; Watts, R. J. *J. Am. Chem. Soc.* **1984**, *106*, 6647–6653.
(10) Sajoto, T.; Djurovich, P. I.; Tamayo, A. B.; Oxgaard, J.; Goddard, W. A.; Thompson, M. E. *J. Am. Chem. Soc.* **2009**, *131*, 9813–9822.
(11) Sajoto, T.; Djurovich, P. I.; Tamayo, A.; Yousufuddin, M.; Bau, R.; Thompson, M. E.; Holmes, R. J.; Forrest, S. R. *Inorg. Chem.* **2005**, *44*, 7992–8003.
(12) Lamansky, S.; Djurovich, P. I.; Murphy, D.; Abdel-Razzaq, F.; Lee, H.-F.; Adachi, C.; Burrows, P. E.; Forrest, S. R.; Thompson, M. E. *J. Am. Chem. Soc.* **2001**, *123*, 4304–4312.
(13) Lowry, M. S.; Hudson, W. R.; Pascal, R. A.; Bernhard, S. *J. Am. Chem. Soc.* **2004**, *126*, 14129–14135.
(14) Lo, K. K. W.; Chan, J. S. W.; Lui, L. H.; Chung, C. K. *Organometallics* **2004**, *23*, 3108–3116.
(15) Tang, C. W.; VanSlyke, S. A.; Chen, C. H. *J. Appl. Phys.* **1989**, *65*, 3610–3616.
(16) Slinker, J. D.; Koh, C. Y.; Malliaras, G. G.; Lowry, M. S.; Bernhard, S. *Appl. Phys. Lett.* **2005**, *86*, 173506.
(17) Tamayo, A. B.; Garon, S.; Sajoto, T.; Djurovich, P. I.; Tsyba, I. M.; Bau, R.; Thompson, M. E. *Inorg. Chem.* **2005**, *44*, 8723–8732.
(18) Graber, S.; Doyle, K.; Neuburger, M.; Housecroft, C. E.; Constable, E. C.; Costa, R. D.; Orti, E.; Repetto, D.; Bolink, H. J. *J. Am. Chem. Soc.* **2008**, *130*, 14944–14945.
(19) Su, H. C.; Chen, H. F.; Wu, C. C.; Wong, K. T. *Chem.—Asian J.* **2008**, *3*, 1922–1928.
(20) Nazeeruddin, M. K.; Humphry-Baker, R.; Berner, D.; Rivier, S.; Zuppiroli, L.; Graetzel, M. *J. Am. Chem. Soc.* **2003**, *125*, 8790–8797.
(21) Li, J.; Djurovich, P. I.; Alleyne, B. D.; Yousufuddin, M.; Ho, N. N.; Thomas, J. C.; Peters, J. C.; Bau, R.; Thompson, M. E. *Inorg. Chem.* **2005**, *44*, 1713–1727.

"Soft salt" is a term introduced to describe ionic materials that are composed of only organometallic components, lacking halide, alkali metal, or other ions commonly present as counterions for these materials.[23] These salts are considered "soft", because their component ions are of significantly larger radii than simple ions so that the lattice energies are expected to be lower and the ions are bonded mainly through van der Waals force. Soft salts can be readily obtained in crystalline form,[24,25] and various cluster ions and soft salts with different metals, such as Fe,[26] Cr,[27] Mo,[28] Os,[29] and Ru,[29] have been studied. De Cola et al., have recently reported the crystal structure of an Ir-based soft salt, closely related to one of the compounds discussed herein.[30]

Mononuclear Ir-based soft salts have not been examined and are interesting alternatives in OLEDs to the neutral materials that have been explored extensively in this application. These soft salts can be easily synthesized through metathesis reactions and show dual emission in solution, ambipolar charge conduction and good flexibility in setting the HOMO and LUMO energy levels, due to the two independent functional components in oppositely charged ions. Herein, we present the synthesis, characterization, and OLED studies for three soft salts. We show that the alignment of the energy levels within the soft salt can be adjusted by the ligand choice for each of the ions and this energy alignment is a critical parameter controlling the performance of the OLED.

Results and Discussion

The ionic Ir complexes were synthesized by refluxing bis-cyclometalated Ir(III) dichloro-bridged dimer in the presence of an excess of an auxiliary ligand, eq 1. The net charge of the resulting Ir complex depends on the auxiliary ligand selected. For example, when cyanide ions are present, two anions coordinate with Ir to generate stable anionic Ir complexes. On the other hand, when neutral ligands, such as diimines and isocyanides, are used, cationic complexes are obtained. By mixing two oppositely charged Ir complexes in water, the soft salts were obtained through a simple metathesis reaction, in moderate yield. The three soft salts studied in this paper are composed of two different cations and three different anions. These five ions are abbreviated based on their charge, namely **C** for cations and **A** for anions, followed by a number to differentiate different ions. The structures of the ions and soft salts and their corresponding acronyms are illustrated in Figure 1.

$$^{1/2}[(C\hat{}N)_2Ir(\mu\text{-}Cl)_2Ir(C\hat{}N)_2] + \text{excess } X^- \text{or } L \rightarrow Cl^- \text{ and } (C\hat{}N)_2IrX_2^- \text{ or } (C\hat{}N)_2IrL_2^+ \quad (1)$$

Photophysics and Quenching Study. The emission data of the ions and soft salts are summarized in Table 1. The photoluminescent (PL) spectra of the ion **C2** and **A3** in degassed acetonitrile solution are presented in Figure 2a as an example. The emission spectrum of **A3,** which peaks at around 450 nm, is blue-shifted by the electron-withdrawing fluorines in the chelating ligand with well-resolved vibronic structure. The structured emission is the result of a triplet ligand-centered (^{3}LC) transition on the cyclometalating ligands.[21] The rest of the ions exhibit a broad and featureless spectrum, similar to that of **C2** in Figure 2a. Single-chelate complexes **C1**, **A1**, and **A2** are all expected to emit from metal-to-ligand charge-transfer (MLCT) states, while the difference in C^N ligand is responsible for the shift in peak position.[31,32] The mixed-ligand complex **C2** showed a significantly red-shifted emission compared to **C1** and **A1**, because Ir→bipyridine (bpy) CT transition, rather than Ir→tolylpyridine (tpy), is the lowest-energy one in this case.[33]

The PL spectra of the soft salts show interesting concentration dependence, a result of one ion quenching the emission of the other. **C2A3** serves as a good example with the distinct spectrum from two ions. PL spectra measured at different concentrations are compared in Figure 2b. On the basis of the spectra, the ratio of two peaks varies greatly depending on the solution concentra-

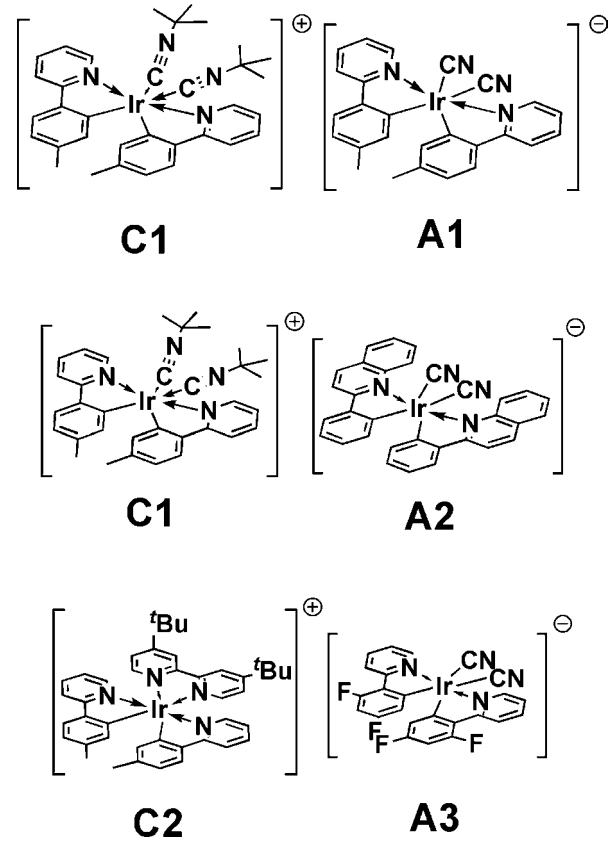

Figure 1. Structure of the soft salts reported here.

(22) Di Censo, D.; Fantacci, S.; De Angelis, F.; Klein, C.; Evans, N.; Kalyanasundaram, K.; Bolink, H. J.; Gratzel, M.; Nazeeruddin, M. K. *Inorg. Chem.* **2008**, *47*, 980–989.
(23) Green, M. L. H.; Hamnett, A.; Qin, J.; Baird, P.; Bandy, J. A.; Prout, K.; Marseglia, E.; Obertelli, S. D. *J. Chem. Soc., Chem. Commun.* **1987**, 1811–1814.
(24) Basolo, F. *Coord. Chem. Rev.* **1968**, *3*, 213–223.
(25) Braga, D.; Grepioni, F. *Organometallics* **1992**, *11*, 711–718.
(26) Toan, T.; Teo, B. K.; Ferguson, J. A.; Meyer, T. J.; Dahl, L. F. *J. Am. Chem. Soc.* **1977**, *99*, 408–416.
(27) Pasynskii, A. A.; Eremenko, I. L.; Rakitin, Y. V.; Novotortsev, V. M.; Ellert, O. G.; Kalinnikov, V. T.; Shklover, V. E.; Struchkov, Y. T.; Lindeman, S. V.; Kurbanov, T. K.; Gasanov, G. S. *J. Organomet. Chem.* **1983**, *248*, 309–320.
(28) Bandy, J. A.; Davies, C. E.; Green, M. L. H.; Green, J. C.; Prout, K.; Rodgers, D. P. S. *J. Chem. Soc., Chem. Commun.* **1983**, 1395–1397.
(29) McQueen, A. E. D.; Blake, A. J.; Stephenson, T. A.; Schroder, M.; Yellowlees, L. J. *J. Chem. Soc., Chem. Commun.* **1988**, 1533–1535.
(30) Mauro, M.; Schuermann, K. C.; Prétôt, R.; Hafner, A.; Mercandelli, P. Sironi, A.; De Cola, L. *Angew. Chem., Int. Ed.* DOI: 10.1002.
(31) Colombo, M. G.; Brunold, T. C.; Riedener, T.; Gudel, H. U.; Fortsch, M.; Burgi, H. B. *Inorg. Chem.* **1994**, *33*, 545–550.
(32) Lamansky, S.; Djurovich, P. I.; Murphy, D.; Abdel-Razzaq, F.; Kwong, R.; Tsyba, I.; Botz, M.; Mui, B.; R., B.; Thompson, M. E. *Inorg. Chem.* **2001**, *40*, 1704–1711.
(33) Colombo, M. G.; Hauser, A.; Gudel, H. U. In *Electronic and Vibronic Spectra of Transition Metal Complexes I*, 2nd ed.; Yersin, H., Ed.; Topics in Current Chemistry Series; Springer: Berlin, 1994; Vol. 171, pp 143−171.

Table 1. Redox Potentials, Energy Levels, Lifetimes, and Quantum Yield Data of the Soft Salts and Their Component Ions under Nitrogen

	redox (V) $E_{1/2}^{ox}/E_{1/2}^{re}$	energy levels (eV) HOMO/LUMO	lifetime (μs)[c]	quantum yield (%) solution	quantum yield (%) film[d]	λ_{max} (nm)[c]
C1[a]	1.21[b]/−2.41[b]	−6.3/−1.9	36.7	38	3.7	458
C2[a]	0.83/−1.86	−5.8/−2.6	0.43	21	16	586
A1[a]	0.51/−2.62	−5.3/−1.7	4.0	70	4.8[e]	472
A2[a]	0.52/−2.25	−5.3/−2.1	3.4	78	3.2[e]	572
A3[a]	0.93/−2.63	−5.9/−1.7	4.1	70	7.8[e]	448
C1A1	0.53/−2.37	−5.3/−2.0	12/3.8	87	7.0	470
C1A2	0.55/−2.28	−5.4/−2.1	8.6/3.1	74	13	456, 572
C2A3	0.82/−1.87	−5.7/−2.6	0.43/1.3	24	18	448, 586

[a] The counterion for **C1** is OTf^-, **C2** is Cl^- and Na^+ for all three anions. [b] Reference 21. [c] Measured in acetonitrile at the concentration below 10^{-3} M. [d] Spin-coated from acetonitrile solution at 3000 rpm for 40 s followed by baking under vacuum at 90 °C for 2 h. Measured under nitrogen. [e] The same as footnote d, except dissolved in acetonitrile/DMF mixture solution (20:1).

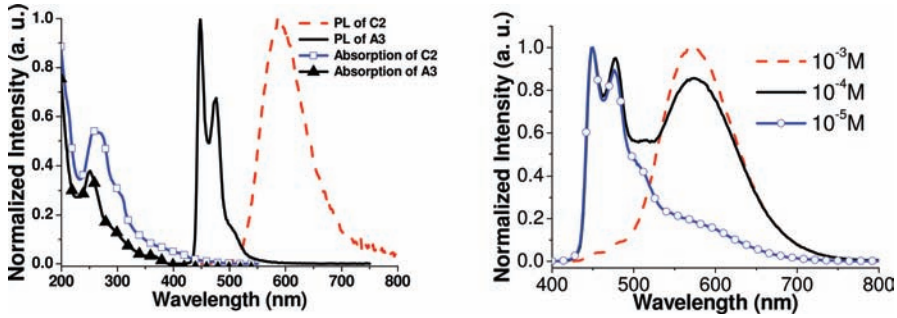

Figure 2. (a) Absorption of **C2**Cl and photoluminescence spectrum of **C2**Cl and **A3**Na; (b) photoluminescence of **C2A3** at different concentrations (all in degassed acetonitrile, excitation wavelength = 350 nm)).

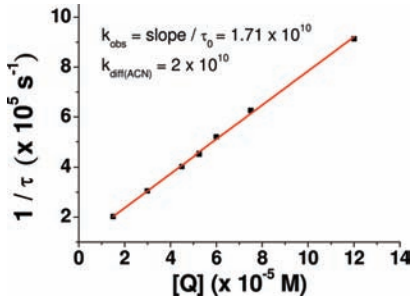

Figure 3. Stern−Volmer plot of the quenching study between **C2** and **A3** and the numerical fitting of K_q.

tion, indicating that the degree of energy transfer between the ions is different. At the relatively low concentration of 10^{-5} M and 350 nm excitation, the emission is mainly from the anion, because the quantum yield of the anion is much larger than that of the cation. This high-energy blue emission diminishes as the solution is concentrated, with cations serving as a quencher of **A3** emission, and exclusive **C2** emission is observed at concentrations of 10^{-3} M and above.

To study the energy transfer between two ions in **C2A3**, Stern−Volmer quenching analysis was carried out. The lifetime of **A3** in degassed acetonitrile solution with various amounts of the quencher, **C2**, was recorded. The concentration of the **A3** was kept at 0.67 μM in all samples and that of the quencher varied from 0 to 120 μM. Based on a bimolecular quenching model, the reciprocal of the lifetime of **A3** is linearly correlated to the concentration of the quencher ([Q] = [**C2**]), as observed for the **C2** and **A3** in Figure 3. The quenching rate constant (K_q) can be extracted by dividing the slope of the fitted straight line by τ_0 (the lifetime with no quencher present). The calculation yields a K_q value of 1.71×10^{10} M^{-1} s^{-1}, close to the diffusion limit in acetonitrile (2×10^{10} M^{-1} s^{-1}).[34] Quenching in **A3** emission occurs by either energy or electron transfer to **C2**.[35] **A3** has a higher phosphorescence energy than **C2**, so energy transfer is a viable pathway for quenching of **A3** emission. While the **A3** emission efficiency and lifetime are decreased in **C2A3** relative to **A3** alone, the values for **C3** are the same as those of **C3** alone (Table 1), suggesting that the energy transfer/quenching process is very efficient. Förster energy transfer is unlikely to be an efficient pathway for energy transfer, because of the poor overlap between the absorption of **C2** and the emission of **A3** (Figure 2a). Electron exchange (Dexter) energy transfer is therefore the likely mechanism of energy transfer in this case.

Quantum Yield and Lifetime. The quantum yields (QY) of the soft salts and their component ions were measured in solution and as neat films (Table 1). In solution, the QYs increased significantly after degassing, consistent with the efficient oxygen quenching of phosphorescence from the complexes. The QYs of degassed solutions of **C1A2** and **C2A3** match the values of the ion with lower energy in the pair, consistent with the efficient energy transfer in soft salts. In films, the QYs are generally lower compared to the values observed in degassed solutions, as expected due to self-quenching. It is interesting to see that the QY values are also sensitive to the size of the ligand and the counterion. For example, soft salts possess higher QYs than their component ions in neat film, because the ions of the soft salts are markedly larger than halide or alkali metal ions, leading to larger intermolecular spacing in the soft salts. Similarly, a bulkier ligand can improve the QY by spacing the ions farther apart in the ionic solids, which explains why **C2**Cl has a higher

(34) Turro, N. J. *Modern Molecular Photochemistry*; University Science Books: Sausalito, CA, 1991; pp 314.
(35) Ma, B.; Djurovich, P. I.; Thompson, M. E. *Coord. Chem. Rev.* **2005**, *249*, 1501–1510.

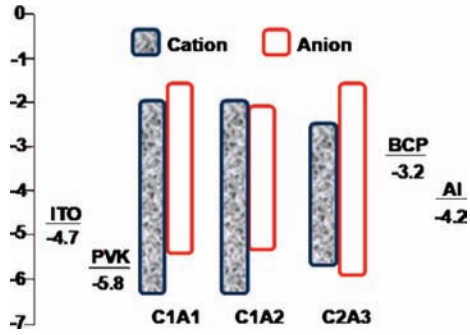

Figure 4. Energy levels of the materials used in the OLEDs.

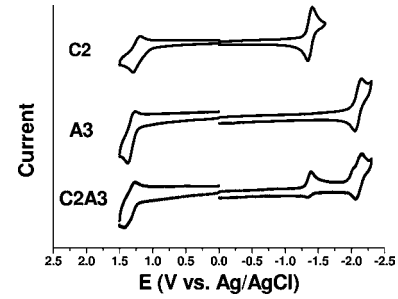

Figure 5. Comparison of cyclic voltammetry between **C2A3** and its component ions.

QY than **C1**Cl in film samples even though their QYs are quite similar in solution.

The lifetime data of the individual ions measured in degassed acetonitrile solution (Table 1) confirm the phosphorescent nature of the photoluminescence. The lifetime measurement for the soft salts all yielded characteristic double-exponential curves, representing different component ions. Because of the quenching through energy transfer, the lifetimes of the component ions with higher triplet energies were all markedly shortened, while the ones with lower energy were not affected.

HOMO and LUMO Energies. The electrochemical properties of the soft salts and individual ions were examined by cyclic voltammetry (CV). The measurements were performed in acetonitrile with ferrocene as the internal reference. HOMO/LUMO levels were obtained from redox potentials using previously published correlations (Table 1).[36,37] The energy levels are also plotted in Figure 4 for comparison purposes. The HOMO/LUMO values of the ions are affected by both the net electrical charge and the chelating ligand. For example, **C1A1** contains two ionic Ir complexes that have the same C^N chelating ligand, leading to very similar emission and absorption energies, while their HOMO and LUMO energy levels differ significantly. The anionic Ir complex (**A1**) is easier to oxidize and harder to reduce than an analogous cationic complex, which translates into a higher HOMO and LUMO than the cation (**C1**).

The HOMO and the LUMO energy of the soft salts are determined by the lowest energy potential in the pair of Ir complexes. The CV of **C2A3** and its component ions are given as an example in Figure 4. The first oxidation and reduction of **C2A3** matches with the oxidation of **A3** and the reduction of the **C2**, respectively. This tunes the energy levels of the soft salts by simply changing the chelating ligands of the individual ions. The idea can be seen by comparing **C1A1** and **C1A2**. **C1A2** is obtained by replacing the tpy group of **A1** with phenylquinoline (PQ) groups, namely **A2**. In **C1A2**, the extended π-conjugation of the PQ ligand lowers the reduction potential more than the positive charge raises it. As a result, **C1A2** has both of its lowest energy potentials on the anion, in contrast to **C1A1** having the lowest energy oxidation and reduction from HOMO of the anion and LUMO of the cation, respectively. Using a similar strategy, the energy levels of **C2A3** were tailored such that oxidation and reduction both take place on the cation. The ability to adjust the energy levels independently allows us to probe the role of carrier trapping on the cationic and anionic component of the soft salt on OLED properties.

OLED Studies. Soft salts were tested in both single layer LEC and heterostructured OLED devices. Typical LECs show slow turn-on time (seconds to minutes), which is a result of gradual charge accumulation at electrode/organic interface, facilitating charge injection. When soft salts were used in an LEC structure (anode/soft salt/cathode), characteristic LEC behavior was not observed. There was no increase in current over a period of 30 min and the devices failed to turn on under voltages ranging from 2.5 to 7 V. This can be explained by the absence of the small ions found in LECs which migrate in the applied electric field, facilitating the charge injection in functional LECs. Charge injection in these soft-salt-based LECs is difficult and imbalanced without the Ohmic contact created by migrating mobile ions to establish a recombination zone in the middle of the soft salt layer. While this simple device structure does not give efficient charge injection into the soft salt materials, carrier transport in the soft salt layer is expected to be the same for both LEC and OLED, namely relying on redox reactions of charged iridium complexes. Being a mixture of cation and anion themselves, soft salts are ambipolar and expected to transport both holes and electrons.

To lower the hole injection barriers in soft-salt-based devices, a polyvinyl carbazole (PVK) layer was spin-coated on the indium tin oxide (ITO). This PVK layer also prevents agglomeration or crystallization of the soft salt layer. The PVK/soft salt layers were capped with a thin film of 2,9-dimethyl-4,7-diphenyl-1,10-phenanthroline to improve energy alignment between the cathode and the soft salts. The energy diagrams for these three soft-salt-based OLEDs are shown in Figure 5. At the interface of PVK and soft salt, the holes are injected by oxidizing the anions and hop between anionic complexes inside the soft salt layer. The charge localization in soft salt layers is quite different from that of the neutral materials typically used in OLEDs. In contrast to the typical OLEDs, where the hole is present as a positive polaron, the hole in the soft salt film forms a neutral species (oxidation of the anion) and the positive charge is delocalized over the lattice, as it is represented by an excess of cations over what is needed for the number of anions. The same is true for the electron, which corresponds to an excess of anions over what is needed to compensate the number of cations in the lattice, after the electron is injected. Charge mobility in the soft salt is expected to be higher than an analogous neutral lattice, due to the higher dielectric of the highly charged soft salt lattice. When a hole and an electron are localized on adjacent molecules, the excess positive and negative lattice charge associated with each carrier are neutralized and the two carriers are expected to be bound, just as

(36) D'Andrade, B. W.; Datta, S.; Forrest, S. R.; Djurovich, P.; Polikarpov, E.; Thompson, M. E. *Org. Electron.* **2005**, *6*, 11–20.
(37) Djurovich, P. I.; Mayo, E. I.; Forrest, S. R.; Thompson, M. E. *Org. Electron.* **2009**, *10*, 515–520.

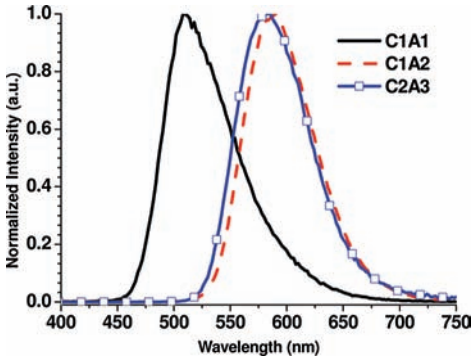

Figure 6. EL of the devices made of three soft salts.

positive and negative polarons can be electrostatically attracted and bound in a neutral lattice.

The electroluminescence (EL) spectra of the devices are shown in Figure 6 and the EQE and $J-V$ characteristics of the devices are compared in Figure 7. The data suggest that the relative position of the energy levels between two ions in the soft salt is crucial to device performance. The component ions of **C1A1** consist of the same cyclometallating ligand, but different ancillary ligands, the latter imparting the charge to the complex. The two ions have similar HOMO/LUMO gaps, but the molecular charges markedly shift the HOMO and LUMO energies. Because the energy barriers between two HOMOs and two LUMOs are both relatively high, it is difficult for carriers to be exchanged between the reduced cation (the electron) and the oxidized anion (the hole), which hinders exciton formation. As a result, there is no obvious preference for recombination to take place on one ionic complex over the other. Although **C1A1** has the lowest PL QY in neat film among three soft salts, the 0.2% EQE of the **C1A1**-based device is far lower than would be expected based on the PL efficiency alone. This suggests that poor matching of the HOMO/LUMO is the principal reason why **C1A1** demonstrates the poorest performance among all three soft salts (Figure 7 and Table 2). In contrast to **C1A1**, **C1A2** and **C2A3** have a close energy match between one of the frontier orbitals, namely close LUMO match for **C1A3** and close HOMO match for **C2A3**. Moreover, in these two soft salts, the energy levels of one ion are bracketed by those of the other, suggesting that one of the ions may carry both the hole and electron. Thus, there is a preference energetically to generate excitons on the ion with the smaller energy gap. The anion of **C1A2** and the cation of **C2A3** serve as a trap for both holes and electrons, which improves the efficiency of exciton formation. The advantage of this energetic configuration is reflected in the markedly higher EQE values for **C1A2** and **C2A3**, that is, 2.6 and 4.7%, respectively (Figure 7a). Compared to the QY data of the films in Table 1, the maximum EQE value of the devices made using **C1A2** and **C2A3** (Table 2) is comparable to the theoretical maximum (the internal efficiency is expected to be 3−5 times higher than EQE).[38]

Table 2. Performance of the OLEDs Made Using Different Soft Salts

	$\lambda_{max,\ EL}$(nm)	$V_{turn\text{-}on}$ (V)	L_{max} (Cd/m^2)	$\eta_{ext,\ max}$ (%)
C1A1	510	4	160 (24 V)	0.2
C1A2	590	3	1971 (24 V)	2.6
C2A3	586	2.5	7428 (21 V)	4.7

Despite the good EQE, the device using **C1A2** shows lower conductivity than the one using **C2A3** (Figure 7b). A similar trend can be seen in the brightness and turn-on voltage data (Table 2). The difference likely stems from the energy barrier for electron injection. The LUMO of the cation of **C1A2** (−1.94 eV) is 0.6 eV higher than that of the cation in **C2A3** (−2.54 eV), creating a larger barrier for electron injection from BCP. In contrast, the effect on hole injection from the energy difference between HOMO of PVK and the HOMO levels of two anions is comparable, based on the energy diagram (Figure 5).

Among the three soft salts, **C2A3** offers the best HOMO/LUMO alignment with hole and electron injection layer, and the energy levels between its component ions also facilitate the charge recombination. The device data for **C2A3**-based OLEDs suggests that soft salts have the potential to prepare OLEDs with properties comparable to those made with neutral Ir phosphors.

Conclusions

Three Ir-based soft salts have been synthesized and characterized. Each soft salt is formed by a pair of ionic Ir complexes, through independently altering the ligands. It is easy to tune the relative energetic properties, which have significant impact on the photophysical, electrochemical and device performance. **C2A3** shows the dual emission in solution, with the ratio of two components in the spectrum dependent on the soft salt concentration. Quenching studies show that the energy transfer process from the blue to red emissive ion is at diffusion controlled limit. The internal alignment between the energy levels of two ions is key to achieve good OLED performance. **C2A3** gives the best overall device performance with the maximal EQE of 4.7%, comparable to the theoretical maximum based on the film PL efficiency. This result suggests that the soft-salt-based devices have the potential to reach efficiencies comparable to neutral Ir-based OLEDs. The key to achieving such high efficiencies is the preparation of soft salts with thin

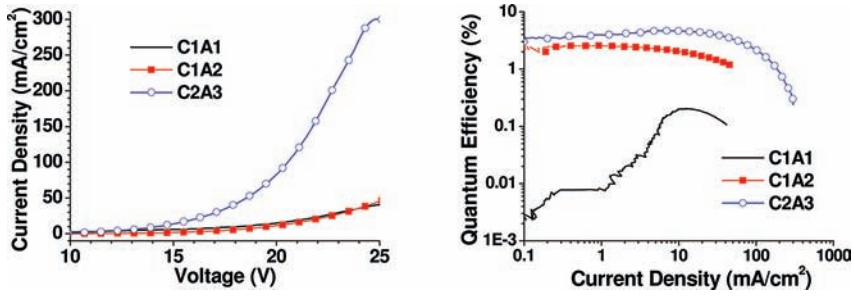

Figure 7. EQE (a) and $J-V$ characteristics (b) of the devices using different soft salts.

film PL efficiencies in the 0.5−1.0 range, which are readily achieved for Ir-phosphor-doped thin films.

Experimental Section

General Experiment. All the starting materials and solvents were purchased from commercial sources and used without further purification. The ^{1}H and ^{13}C NMR spectra were collected on a 400 MHz spectrometer at room temperature. Mass spectra were recorded on an Applied Biosystems Voyager-DE STR mass spectrometer. IR data was obtained from a Perkin-Elmer Spectrum 2000 FT-IR spectrometer. Elemental analyses for the three soft salts were carried out in an Heraeus Vario EL III elemental analyzer at NSC Regional Advanced Instrument Center, National Taiwan University. Samples dried under vacuum at room temperature yielded elemental analyses with higher-than-expected percentage for carbon, consistent with solvent being trapped in the porous crystals.[30] Heating the samples under vacuum overnight at 100 °C gave better CHN analyses (vide infra).

General Procedures for Synthesis. All experiments involving $IrCl_3 \cdot H_2O$ or any other Ir(III) species were carried out in an inert atmosphere. Cyclometalated Ir(III) dichlorobridged dimers were synthesized according to published procedures.[9,39,40] The reaction conditions and purification procedures reported in this paper were not optimized for yield.

[Ir(tpy)$_2$(CN-t-Bu)$_2$]Cl, C1. The characterization was previously published.[21]

[Ir(tpy)$_2$(^{t}bpy)]Cl, C2. A mixture of iridium 2-(*p*-tolyl)pyridine dichloro-bridged dimer (150 mg, 0.13 mmol) and 4,4′-di-*tert*-butyl-2,2′-bipyridine (79 mg, 0.29 mmol) was dissolved in methanol (10 mL) and refluxed for 15 h. The solution was concentrated and washed with hexane to afford pure product (185 mg, 84%) as a yellow solid. ^{1}H NMR (DMSO-d_6, 400 MHz) δ: 8.86 (s, 2H), 8.20 (d, J = 8.0, 2H), 7.90 (td, J = 7.5, 1.4, 2H), 7.80 (d, J = 8.0, 2H), 7.76 (d, J = 5.9, 2H), 7.72 (dd, J = 5.9, 1.9, 2H), 7.55 (d, J = 5.8, 2H), 7.13 (td, J = 6.6, 1.4, 2H), 6.83 (dd, J = 7.9, 1.1 2H), 5.98 (s, 2H), 2.06 (s, 6H), 1.38 (s, 18H). ^{13}C NMR, (DMSO-d_6, 100 MHz) δ: 166.88, 163.43, 155.03, 151.36, 149.41, 148.59, 141.15, 139.52, 138.52, 131.61, 125.43, 124.94, 123.32, 123.10, 122.17, 119.60, 35.64, 29.95, 21.43. MS (MALDI) *m*/*z* 797 (M − Cl).

Na[Ir(tpy)$_2$(CN)$_2$], A1. Iridium 2-(*p*-tolyl)pyridine dichloro-bridged dimer (500 mg, 0.44 mmol) was combined with sodium cyanide (261 mg, 5.32 mmol) in methanol (50 mL) and refluxed with stirring for 15 h. The crude product was purified through column chromatography on silica gel (DMF) to yield pure product (470 mg, 88%) as a light yellow solid. ^{1}H NMR (DMSO-d_6, 400 MHz) δ: 9.48 (d, J = 6.0, 2H), 8.02 (d, J = 8.0, 2H), 7.86 (td, J = 8.0, 1.2, 2H), 7.55 (d, J = 8.0, 2H), 7.26 (td, J = 6.0, 1.2, 2H), 6.55 (dd, J = 8.0, 1.2, 2H), 5.89 (s, 2H), 1.92 (s, 6H). ^{13}C NMR, (DMSO-d_6, 100 MHz) δ: 167.84, 163.98, 153.07, 141.83, 137.00, 135.90, 131.55, 131.07, 123.52, 121.91, 120.95, 118.51, 21.41. IR: 2102, 2088 cm^{-1} (terminal C≡N stretch). MS (MALDI) *m*/*z* 581 (M − Na).

Na[Ir(pq)$_2$(CN)$_2$], A2. Iridium phenylquinoline dichloro-bridged dimer (500 mg, 0.39 mmol) was combined with sodium cyanide (231 mg, 4.71 mmol) in methanol (50 mL) and refluxed with stirring for 15 h. The crude product was purified through column chromatography on silica gel (DMF) to yield pure product (521 mg, 94%) as a light yellow solid. ^{1}H NMR (DMSO-d_6, 400 MHz) δ: 10.13 (d, J = 8.0, 2H), 8.48 (d, J = 8.0, 2H), 8.26 (d, J = 8.0, 2H), 8.04 (dd, J = 8.0, 1.6, 2H), 7.80 (d, J = 8.0, 2H), 7.75 (td, J = 8.0, 1.6, 2H), 7.68 (td, J = 8.0, 1.6, 2H), 6.76 (td, J = 8.0, 1.2, 2H), 6.54 (td, J = 8.0, 1.2, 2H), 5.95 (dd, J = 8.0, 1.2, 2H). ^{13}C NMR, (DMSO-d_6, 100 MHz) δ: 171.46, 166.75, 148.75, 146.91, 138.25, 132.81, 131.52, 130.19, 129.80, 128.80, 127.85, 127.32, 126.17, 125.82, 120.00, 117.64. IR: 2107, 2087 cm^{-1} (terminal C≡N stretch); MS (MALDI) *m*/*z* 653 (M − Na).

Na[Ir(dfppy)$_2$(CN)$_2$], A3. Iridium 2-(2,4-difluorophenyl)pyridine dichloro-bridged dimer (300 mg, 0.25 mmol) was combined with sodium cyanide (145 mg, 2.96 mmol) in methanol (30 mL) and refluxed with stirring for 15 h. The crude product was purified through column chromatography on silica gel (DMF) to yield pure product (270 mg, 84%) as a light yellow solid. ^{1}H NMR (DMSO-d_6, 400 MHz) δ: 9.55 (d, J = 6.0, 2H), 8.22 (d, J = 8.0, 2H), 8.03 (td, J = 8.0, 1.2, 2H), 7.44 (td, J = 6.0, 1.2, 2H), 6.63 (ddd, J = 12.8, 9.6, 2.4, 2H), 5.54 (dd, J = 8.0, 2.4, 2H). ^{13}C NMR, (DMSO-d_6, 100 MHz) δ: 170.2, 163.42, 154.97, 145.83, 139.76, 137.44, 132.17, 129.64, 124.72, 123.36, 121.62, 120.11, 59.49, 24.77, 20.70, 13.93. IR: 2114, 2106 cm^{-1} (terminal C≡N stretch). MS (MALDI) *m*/*z* 625 (M − Na).

C1A1. [Ir(tpy)$_2$(CN)$_2$]OTf (50 mg, 0.07 mmol) and Na[Ir(tpy)$_2$-(CN)$_2$] (50 mg, 0.08 mmol) were added to water (10 mL). The reaction mixture was stirred for 1 h at room temperature and then extracted with CH_2Cl_2. The combined organic extracts were dried over $MgSO_4$ and concentrated by rotary evaporation. The resulting solid was washed with ethyl ether to afford **C1A1** (49 mg, 65%) as a yellow solid. ^{1}H NMR (DMSO-d_6, 400 MHz) δ: 9.48 (d, J = 5.1, 2H), 8.98 (d, J = 5.8, 2H), 8.29 (d, J = 7.9, 2H), 8.17 (td, J = 7.8, 1.4, 2H), 8.00 (d, J = 7.8, 2H), 7.85 (td, J = 7.8, 1.6, 2H), 7.78 (d, J = 8.0, 2H), 7.55 (d, J = 8.0, 4H), 7.51 (td, J = 6.7, 1.5, 2H), 7.25 (td, J = 6.6, 1.4, 2H), 6.80 (dd, J = 7.9, 1.1, 2H), 6.55 (dd, J = 8.4, 1.8, 2H), 5.89 (s, 2H), 5.83 (s, 2H), 1.98 (s, 6H), 1.92 (s, 6H), 1.31 (s, 18H). ^{13}C NMR, (DMSO-d_6, 100 MHz) δ: 167.85, 166.60, 164.05, 153.30, 153.13, 153.10, 141.85, 141.28, 139.50, 139.23, 136.99, 135.88, 131.57, 131.01, 130.35, 124.82, 124.52, 124.13, 123.51, 121.91, 120.94, 120.43, 118.50, 94.48, 58.52, 29.51, 21.42; IR: 2187, 2161, 2101, 2093 cm^{-1} (terminal C≡N stretch). MS (MALDI) *m*/*z* 695 (M^+), 581 (M^-). Anal. Calcd. for $C_{60}H_{58}Ir_2N_8 \cdot 2H_2O$: C, 54.94; H, 4.76; N, 8.54. Found: C, 54.62; H, 4.75; N, 8.32.

C1A2. [Ir(tpy)$_2$(CN)$_2$]OTf (80 mg, 0.09 mmol) and Na[Ir(pq)$_2$-(CN)$_2$] (80 mg, 0.11 mmol) were added to water (15 mL). The reaction mixture was stirred for 1 h at room temperature and then extracted with CH_2Cl_2. The combined organic extracts were dried over $MgSO_4$ and concentrated by rotary evaporation. The resulting solid was washed with ethyl ether to afford **C1A2** (85 mg, 67%) as a yellow solid. ^{1}H NMR (DMSO-d_6, 400 MHz) δ: 10.13 (d, J = 8.8, 2H), 8.98 (d, J = 6.1, 2H), 8.46 (d, J = 8.6, 2H), 8.28 (d, J = 7.9, 2H), 8.24 (d, J = 9.0, 2H), 8.17 (td, J = 8.1, 1.5, 2H), 8.01 (dd, J = 7.9, 1.6, 2H), 7.78 (d, J = 8.0, 4H), 7.72 (td, J = 7.8, 1.7, 2H), 7.66 (td, J = 7.4, 1.1, 2H), 7.51 (td, J = 6.6, 1.5, 2H), 6.80 (dd, J = 7.9, 1.1, 2H), 6.73 (td, J = 7.2, 1.3, 2H), 6.51 (t, J = 7.3, 2H), 5.93 (d, J = 7.6, 2H), 5.84 (s, 2H), 1.98 (s, 6H), 1.30 (s, 18H). ^{13}C NMR, (DMSO-d_6, 100 MHz) δ: 171.42, 166.79, 166.57, 153.20, 153.02, 148.74, 146.86, 141.21, 139.44, 139.11, 138.15, 132.81, 131.50, 130.31, 130.08, 129.69, 128.71, 127.75, 127.27, 126.08, 125.72, 124.72, 124.38, 124.05, 120.35, 119.92, 117.54, 58.43, 29.47, 21.33; IR: 2183, 2159, 2105, 2088 cm^{-1} (terminal C≡N stretch). MS (MALDI) *m*/*z* 695 (M^+), 653 (M^-). Anal. Calcd. for $C_{66}H_{58}Ir_2N_8 \cdot 2H_2O$: C, 57.29; H, 4.52; N, 8.10. Found: C, 57.29; H, 4.63; N, 8.04.

C2A3. [Ir(tpy)$_2$(^{t}bpy)]Cl (83 mg, 0.10 mmol) and Na[Ir(dfppy)$_2$-(CN)$_2$] (80 mg, 0.12 mmol) were added to water (15 mL). The reaction mixture was stirred for 1 h at room temperature and then extracted with CH_2Cl_2. The combined organic extracts were dried over $MgSO_4$ and concentrated by rotary evaporation. The resulting solid was washed with ethyl ether to afford **C2A3** (90 mg, 64%) as a yellow solid.^{1}H NMR (DMSO-d_6, 400 MHz) δ: 9.54 (dd, J = 4.8, 1.0, 2H), 8.85 (s, 2H), 8.19 (d, J = 7.5, 4H), 8.03 (td, J = 8.3, 1.3, 2H), 7.90 (td, J = 8.2, 1.5, 2H), 7.80 (d, J = 8.0, 2H), 7.76 (d, J = 5.9, 2H), 7.71 (dd, J = 5.9, 1.9, 2H), 7.55 (d, J = 5.8, 2H), 7.44 (td, J = 6.6, 1.4, 2H), 7.12 (td, J = 6.7, 1.4, 2H), 6.84 (dd, J = 8.3, 1.3, 2H), 6.60 (ddd, J = 13.0, 9.4, 2.5, 2H), 5.98 (s, 2H), 5.52 (dd, J = 8.3, 2.5, 2H), 2.06 (s, 6H), 1.38 (s, 18H). ^{13}C NMR, (DMSO-d_6, 100 MHz) δ 166.88, 163.43, 155.03, 151.36, 149.41, 148.59, 141.15, 139.52, 138.52, 131.61, 125.43, 124.94, 123.32,

(38) Hung, L. S.; Chen, C. H. *Mater. Sci. Eng., R* **2002**, *39*, 143–222.
(39) Lohse, O.; Thevenin, P.; Waldvogel, E. *Synlett* **1999**, *1*, 45.
(40) Nonoyama, M. *Bull. Chem. Soc. Jpn.* **1974**, *47*, 767.

123.10, 122.17, 119.60, 35.64, 29.95, 21.43. IR: 2113, 2106 cm^{-1} (terminal C≡N stretch). MS (MALDI) *m/z* 797 (M^+), 625 (M^-). Anal. Calcd. for $C_{66}H_{56}F_4Ir_2N_8 \cdot H_2O$: C, 55.06; H, 4.06; N, 7.78. Found: C, 55.06; H, 4.57; N, 7.65.

Characterization Methods. Oxidation and reduction potentials were measured by cyclic voltammetry (CV). CV scans were recorded at a scan rate of 100 mV/s in dry and degassed acetonitrile with 0.1 M tetrabutylammonium hexafluorophosphate as electrolyte. Ferrocene/ferrocenium (Cp_2Fe/Cp_2Fe^+) redox couple was used as an internal reference. A Pt wire and a glassy carbon rod were used as the counterelectrode and the working electrode, respectively. An Ag wire was also used as a pseudoreference electrode.

The quenching study applied to determine the bimolecular quenching rate constants is calculated according to

$$\tau_0/\tau = 1 + K_q\tau_0[Q] \quad (1a)$$

where τ and τ_0 are the excited state lifetime with and without the quencher, K_q is the experimental quenching rate constant and [Q] is the molar concentration of the quencher. All the sample solutions for the quenching study had the same concentration for the emitter, **A3**, at 0.67 μM. The concentration of the quencher, **C2**, ranged from 0 to 120 μM. Lifetime measurements were performed on an IBH lifetime system after all the solution samples were bubble-degassed with nitrogen for 5 min and excited at 380 nm.

Both photoluminescence (PL) and electroluminescence (EL) emission spectra were obtained by a PTI QuantaMaster model C-60SE spectrofluorometer, equipped with a 928 PMT detector and corrected for detector response. Acetonitrile was used as solvent for solution PL. Films used for obtaining PL spectra and quantum yield were spin-coated on quartz substrates in air at room temperature from acetonitrile solutions. Quantum yield was measured by a Hamamatsu PL Quantum Yield Measurement System (C9920-01).

Device (OLED) Fabrication and Testing. The OLEDs were grown on precleaned ITO-coated glass substrates with sheet resistance of 20 Ω /sq. A 20 mg portion of PVK was dissolved in 1 mL dichlorobenzene and filtered before being spin-coated onto ITO at a rate of 3000 rpm for 40s, followed by baking at 90 °C for 1 h under vacuum. The soft salts were then spin-coated from the acetonitrile solution (30 mg/mL) before the baking under the same conditions. Thereafter, the substrates were transferred to the vacuum chamber where the BCP layer was deposited by thermal evaporation from a resistively heated tantalum boat at a rate of around 2 Å/s. A shadow mask was placed on the substrates and the cathode consisting of 10 Å of LiF and 1200 Å of Al was subsequently deposited. The devices were tested in air within 1 h after fabrication. Light coming out from the front surface was collected by a UV-818 Si photocathode leading to a Keithley 2400 SourceMeter/2000 multimeter coupled to a Newport 1835-C optical meter. Device current−voltage and light-intensity characteristics were measured using the LabVIEW program by National Instruments.

Acknowledgment. The authors thank Universal Display Corp. (UDC) for financial support to this project and Thin Film Devices Inc. for ITO-coated substrates. Hsiao-Fan Chen thanks the National Science Council of Taiwan for the financial support (NSC-096-2917-I-002-128).

Supporting Information Available: Additional photophysical data (lifetimes and photoluminescence spectra) and CV data of soft salts and their component ions. This material is available free of charge via the Internet at http://pubs.acs.org.

JA9097725